Journal of Nondestructive Evaluation (2018) 37:26
https://doi.org/10.1007/s10921-018-0480-6

Non-destructive Flaw Mapping of Steel Surfaces by the Continuous Magnetic Barkhausen Noise Method: Detection of Plastic Deformation

Freddy Armando Franco Grijalba[1] · **Linilson Rodrigues Padovese**[2]

Received: 22 December 2016 / Accepted: 15 March 2018 / Published online: 19 March 2018

Abstract
This paper reports the use of a non-destructive scanning technique to identify plastic deformation defects generated in steel. The technique is based on measurement of continuous magnetic Barkhausen noise (CMBN). In the experiments described here, surfaces with plastic deformations produced by crushing stresses in a 1070 steel are scanned, and the influence of probe configuration, coil type, scanner speed, applied magnetic field and the frequency band used for the analysis on the effectiveness of the technique is studied. A moving smoothing window based on a second order statistical moment is used to analyze the time signal. The results show that the method can detect the position of plastic deformation defects and distinguish between their amplitudes.

Keywords Continuous Barkhausen noise · Surface scanning · Plastic deformation

1 Introduction

Measurement of magnetic Barkhausen noise (MBN) is a non-destructive testing (NDT) technique that has been studied for the last two decades, and suitable applications, equipment and measuring procedures continue to be the subject of research [1–3]. MBN was discovered by Henry Barkhausen in 1919 [4] when he was working on experiments with earphones. He found that when ferromagnetic materials are magnetized by variable fields, a "noise" can be detected in the voltage induced in a pickup coil placed near the material; this is called Barkhausen noise. It has been shown that magnetic emissions, which can be detected by a coil as a series of voltage pulses, are generated by reversible and irreversible movements of the 90° and 180° magnetic domain walls and by domain rotation [5].

MBN is known to be sensitive to several material and mechanical properties, such as grain size [6–8], carbon content [9], stress state [10,11], hardness [12] and plastic deformation [13,14], and its potential for use in the non-destructive measurement of metallurgical, microstructural and mechanical parameters has therefore been the subject of study.

Traditionally, MBN signals are measured with a probe consisting of a magnetic excitation system (magnetizing yoke) and an MBN sensor (pickup coil) (Fig. 1a). Cyclic magnetic excitation is generated in the material, and the Barkhausen noise is measured by the sensor. Barkhausen noise is not produced uniformly throughout the magnetization cycle but is concentrated in two bursts of activity per cycle near the coercive field. As this implies that the probe needs to be kept still on the surface for at least half an excitation cycle when measurements are being taken, the traditional method of measuring Barkhausen noise can be considered a "stationary MBN technique". The use of cyclic magnetic excitation for continuous surface scanning using Barkhausen noise therefore has some drawbacks.

When a magnet is moved over a ferromagnetic sample, the constant sliding magnetic field also produces a time-varying magnetic field in the material. If this magnetic field is strong enough, it will produce Barkhausen emissions, and a pickup coil placed close to the magnetic source will detect Barkhausen noise continuously. This signal is known as continuous magnetic Barkhausen noise (CMBN) and was originally studied by Crouch [15,16]. Few other studies of CMBN have been published.

✉ Freddy Armando Franco Grijalba
frefranco@fem.unicamp.br; frefranco@gmail.com

[1] Faculty of Mechanical Engineering, University of Campinas, Rua Mendeleyev, 200, Campinas 13083-860, Brazil

[2] Department of Mechanical Engineering, Engineering School, University of São Paulo, Av. Prof. Mello Moraes, 2231, São Paulo 05508-900, Brazil

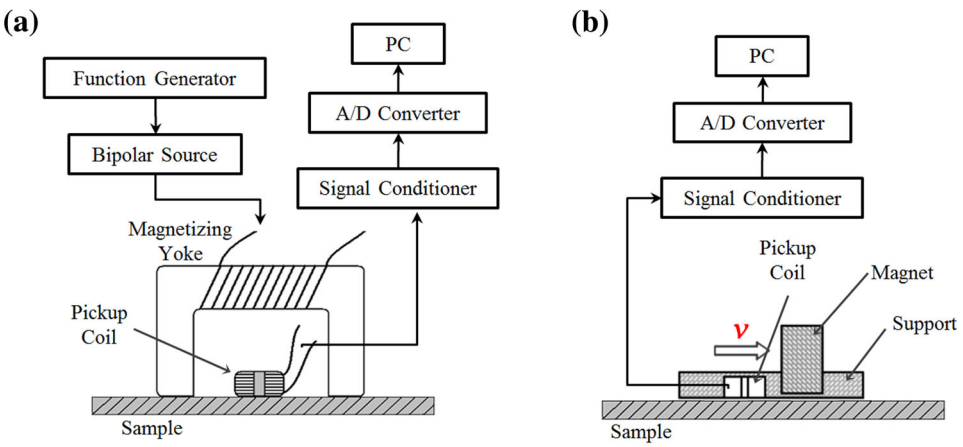

Fig. 1 Schematic diagrams of the measurement systems used for the two techniques: stationary MBN (**a**) and CMBN (**b**)

A previous study by our research group showed how CMBN can be applied to volumetric flaw mapping [17] to detect the size and thickness of artificial grooves produced in a 1070 steel. The influence of probe configuration, scanning speed and the frequency band used for the analysis on the effectiveness of the technique was studied, and the magnetic behavior of the probe was analyzed by numerical simulation using the finite element method (FEM). The results showed that the presence of a ferrite core in the coil favors the emission and detection of CMBN. Another study by our group described a device that uses permanent magnets to create a precise rotating magnetic field [18]. The MBN pickup coil is fixed in the center of the rotating magnetic field, and the device measures CMBN signals as the angle of magnetization varies to determine the direction of the macroscopic magnetic easy axis.

Some characteristics of stationary MBN and CMBN techniques are compared in Table 1.

This paper seeks to provide a greater understanding of the potential applications of the CMBN measurement technique by showing how this scanning method can be used to detect plastic deformation of steel surfaces. The influence of different variables (probe configuration, pickup coil, scanner speed, applied magnetic field and the frequency band used for the analysis) on the effectiveness of the technique is investigated. The results support the use of MBN for nondestructive flaw mapping of steels.

2 Experimental Setup

The AISI 1070 steel sample used measured 27 × 240 × 3mm. Its chemical composition (wt%) was 0.67C, 0.22Si, 0.003S, 0.69Mn, 0.018P and 0.043Al. To eliminate possible residual stresses generated in the rolling process, the sample was subjected to heat treatment at 850°C for 4 h in a controlled atmosphere. The yield limit of the material after heat treatment was 310 MPa. Two regions with different levels of plastic deformation were generated on the surface of the sample by applying compressive loads with a 65mm-diameter steel cylinder. Figure 2 shows the loads used to produce each of the deformations and their positions on the sample. A low-speed grinding process with liquid cooling was then used to eliminate any variations in thickness in the sample generated by the compressive loads and any consequent variations in magnetic flux, as these could lead to errors when interpreting the measurements. The sample had a uniform final thickness of 2.75 mm.

The CMBN probe consisted of a magnet, which produces the constant field referred to earlier, and a coil with a ferrite core to measure the MBN. The probe is shown in Fig. 3. The characteristics of the coil, applied magnetic field, scanning speed and orientation of the probe in relation to its movement were varied during the experiments. The characteristics of the various coils, which were wound with 0.05 mm diameter wire, are shown in Fig. 4 and Table 2. Neodymium iron boron magnets measuring 16 × 12 × 5 mm were used in stacks 1, 2, 3 and 4 magnets high to generate magnetic flux densities of 0.26T, 0.36T, 0.41T and 0.45T, respectively (these values were obtained using a gauss-meter and the magnets were in the air). Scanning speeds of 9, 13, 23 and 33 mm/s were used, and the coil was placed in front of or behind the magnets. (The position of the coils is defined in relation to the direction in which the magnet is being moved.)

The probe was kept in a fixed position during the experiments and the samples were moved under it on an xyz table. The signal was measured with equipment developed in our laboratory that first amplifies it and then filters it in a 1–100 kHz bandpass filter. The sampling frequency was 200 kHz. The xyz table and measurements were controlled by a computer. Measurements were taken six times with each configuration.

Since the inspection technique presented in this paper uses the principle of surface scanning, the signal analysis procedure had the objective of generating a signal amplitude profile that would allow to identify the position of the flaw on the

Table 1 Comparison of stationary MBN and CMBN techniques

	Stationary MBN technique	CMBN technique
Measurement procedure	The measurement process is discrete, and point-to-point measurements are made on the surface of the material. While the Barkausen signals are being measured and recorded by the system, the probe must be kept still on the surface	The measurement process requires the probe to be moved at constant speed over the surface of the material. The method can therefore be considered a surface scanning technique
Experimental setup	The applied magnetic field is an alternating field controlled by electromagnets (magnetizing yoke). A bipolar current or voltage source is therefore essential in the experimental setup. (See Fig. 1a.). The current source is the largest component of the measurement system	As the applied magnetic field can be generated by magnets, the experimental setup does not need to use bipolar current sources. (See Fig. 1b). The measurement system is thus simpler than that required when the stationary MBN technique is used
Change of magnetic domains and amplitude of the Barkhausen noise	The material is subjected to complete magnetization cycles (i.e., complete cycles of the magnetic hysteresis curve). The dynamics of the movement of the domain walls is stronger, and the amplitude of the Barkhausen signal is therefore greater	The changes in the magnetic domains are generated simultaneously by the variation in amplitude and direction of the magnetic flux, which are a consequence of the relative velocity of the probe and sample. The material is not subjected to complete magnetization cycles. The dynamics of the movement of the domain walls is relatively weak, and the Barkhausen signals are consequently smaller than those generated with the stationary MBN technique
Sensor design	The sensor consists essentially of an electromagnet (yoke) to induce the magnetic flux in the sample and a pickup coil placed near the surface of the material that measures the Barkhausen signal (see Fig. 1a)	The sensor is composed of a magnet and a pickup coil with a ferrite core. The pickup coil has the same characteristics as that used with the stationary MBN technique (see Figs. 1b, 3)
Signal characteristics	In each magnetization cycle two Barkhausen signal bursts are generated. These are generated near the Hc region of the magnetic hysteresis cycle. In the region close to positive or negative magnetic saturation of the material, the MBN signal generation is minimal or almost zero	The Barkhausen signal is continuously generated and measured as the probe moves over the material surface. The burst characteristic of the signal generated when the stationary MBN technique is used is not present. Instead, there is a continuous signal whose amplitude varies where the sample is damaged (see Fig. 5)
Interpretation	The MBN signal (which consists of one or more recorded bursts) is generated by, and therefore reflects the characteristics of, a small volume of material extending from the surface of the sample to a depth of approximately 1.5 mm. The measurement is made at a point on the surface of the sample. The surface area measured is proportional to the area of the pickup coil. Statistical parameters of the signal or the shape of the signal envelope are analyzed	The measurement is made along a line on the surface of the sample, and the CMBN signal is generated by, and reflects the characteristics of, a volume of material extending approximately 1.5 mm below the line. The result of the data analysis is a profile of the signal amplitude that reflects the position of the damage in the sample. The profile is determined by calculating parameters for selected data sets with sliding time windows

inspected surface. Thus, two methods of CMBN signals processing were used, as presented in [17]. The first involves calculating the parameter $M2_{CMBN}$, given by:

$$M2_{CMBN}[i] = \frac{1}{2M+1} \sum_{j=-M}^{M} s^2[i+j] \tag{1}$$

where 2M is the size of the sliding time window and s[i] is the CMBN signal. The parameter $M2_{CMBN}$ represents the signal amplitude profile, which allows to identify the flaws positions. In this calculation the signal can be pre-filtered in certain analysis frequency bands that may be more sensitive to the detection of a certain flaw. For the identification of these possible frequency bands, a second method of analysis is used; this involves a time-frequency representation known as a spectrogram. The spectrogram of a signal $x(t)$ is referred to as $SPEC$(t,f) and is given by:

$$\begin{aligned} SPEC(\text{t,f}) &= |STFT(\text{t,f})|^2 \\ &= \left| \int_{-\infty}^{\infty} x(\tau) h^*(\tau - t) e^{-j2\pi f \tau} d\tau \right|^2 \end{aligned} \tag{2}$$

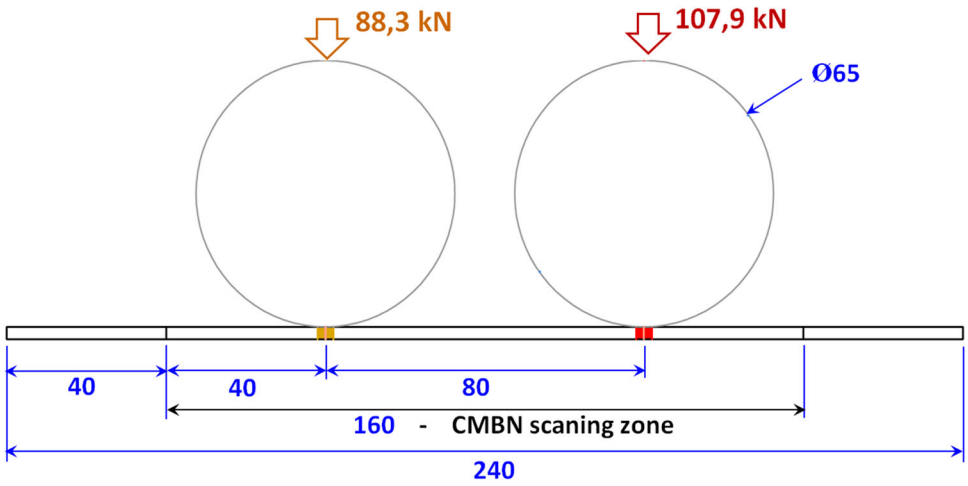

Fig. 2 Position of the plastic deformations in the sample (dimensions in mm)

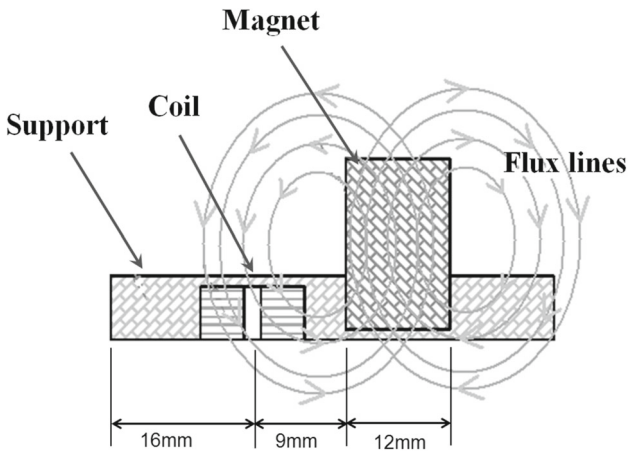

Fig. 3 Schematic diagram of CMBN probe in the air

where h(t) is a weighted sliding window whose width determines the frequency and time resolution, and the superscript * denotes the conjugate. *STFT(t,f)* is the short-time Fourier transform, where t is the time variable and f the frequency variable. Further information on the signal analysis procedure can be found in [17].

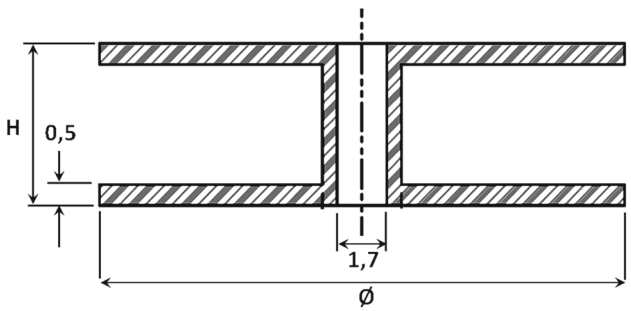

Fig. 4 Geometry of coils used in CMBN probe (dimensions in mm)

Table 2 Characteristics of the different coils used in CMBN probe

Coil	No. of turns	Ø (mm)	H (mm)
A	1250	7	5
B	2000	14	4
C	2500	10	5
D	4000	18	3

3 Results and Discussion

3.1 The Effect of Probe Configuration

Figure 5 shows examples of CMBN time signals for two types of coils used in the probe. When represented in this way without any processing, these signals do not provide any information that allows damage to the sample to be identified.

The variation in $M2_{CMBN}$ along the sample for the four coils used is shown in Fig. 6. These results were obtained using one magnet, a scanning speed v = 33 m/s and each of the coils in turn placed behind the magnet. Each line is the average of six signals, and as in the previous study by our research group [17], the standard deviation of each group of six signals was less than 5%, indicating the acceptable reproducibility of the measurements. Figure 6 shows that none of the coils yielded acceptable results when a frequency band from 1 to 100 kHz was used for the signal analysis.

As shown in [17], there is a significant improvement in flaw detection when suitable signal processing is used. With the aid of spectrograms, for example, signal frequency bands that are more sensitive in terms of flaw detection can be identified. The spectrograms of the CMBN signals measured along the sample with each of the coils are shown in Fig. 7.

The spectrograms show that the best response is obtained with coil A. With this coil, smaller-amplitude transients corresponding to the positions of the plastic deformations in the

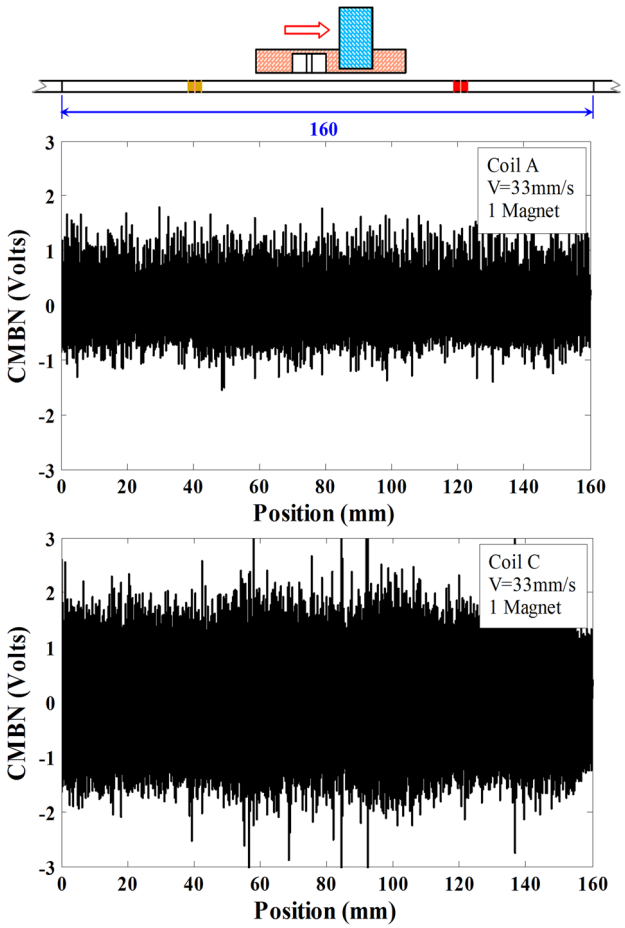

Fig. 5 Examples of CMBN signals

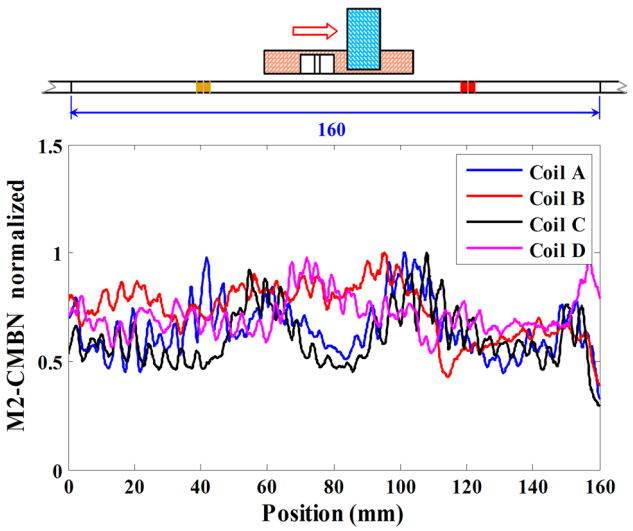

Fig. 6 Normalized variation in $M2_{CMBN}$ along the sample with a 1–100 kHz analysis band. Results using four different coils and one magnet in the probe with a scanning speed v = 33 mm/s

sample can be seen. These transients are not clearly identifiable when the other coils are used. Although coil D has more turns (4000) than coil A (1250) and therefore produces larger-amplitude signals, it yields worse results.

When MBN or CMBN is being measured, the ability of the coil to detect a particular type of flaw, in this case plastic deformation, depends not only on the amplitude of the signals measured but also on certain electrical characteristics (resistance, inductance and capacitance) that affect its response and resonant frequency [19–22]. These characteristics are influenced by the type of wire used to manufacture the coil, the number of turns and the winding arrangement (whether the coil is short or long). Coils with more turns produce greater-amplitude signals and have lower resonant frequencies, while coils with fewer turns produce smaller-amplitude signals and have higher resonant frequencies. The type of coil used is therefore very important.

The resonant frequencies of the coils used in this study can be identified by the signal intensity in the spectrograms in Fig. 7. For coils B, C and D the resonant frequencies are approximately 75, 58 and 25 kHz, respectively, while for coil A the resonant frequency lies above the signal analysis frequency (100 kHz).

Narrow bands of stationary frequencies close to 30 kHz and below 10 kHz can also be seen. This is electromagnetic interference detected by the coils or the electronic equipment. It is unrelated to Barkhausen emissions and can be eliminated with a bandpass filter. When a 30–100 kHz bandpass filter is used and $M2_{CMBN}$ is calculated, the graph in Fig. 8 is obtained, showing that the plastic deformation zones can now be much more clearly identified.

The results in Fig. 8 corroborate the comments related to Fig. 7, i.e., that the best response is obtained with coil A. Although coil D produces greater-amplitude signals because it has more turns (4000), its resonant frequency is close to the region where the interference occurs. The greater amplitude of the signals produced with this coil can therefore be explained by the interference. The coil's ability to detect plastic deformations is, in contrast, minimal. Although coils B and C yielded better results, they were not as effective in detecting flaws as coil A. One reason for this is that because of their larger diameters (Ø 14 mm and Ø 10 mm, respectively), these coils scan larger areas than coil A (Ø 7 mm). Thus, the instantaneous signals generated by coils B and C come from larger volumes of material than those detected by coil A. The scanning resolution and, consequently, sensitivity of coil A is therefore higher.

Figure 8 shows that the CMBN technique can detect the positions of the two plastic deformation zones and distinguish between their amplitudes and that the Barkhausen signal decreases with increasing plastic deformation. As shown in item 2 (experimental setup), plastic deformations were generated by contact stresses (Hertz contact stress) by pressing a cylinder on a flat surface (the sample). Additionally, according to the classic theoretical formulation that shows

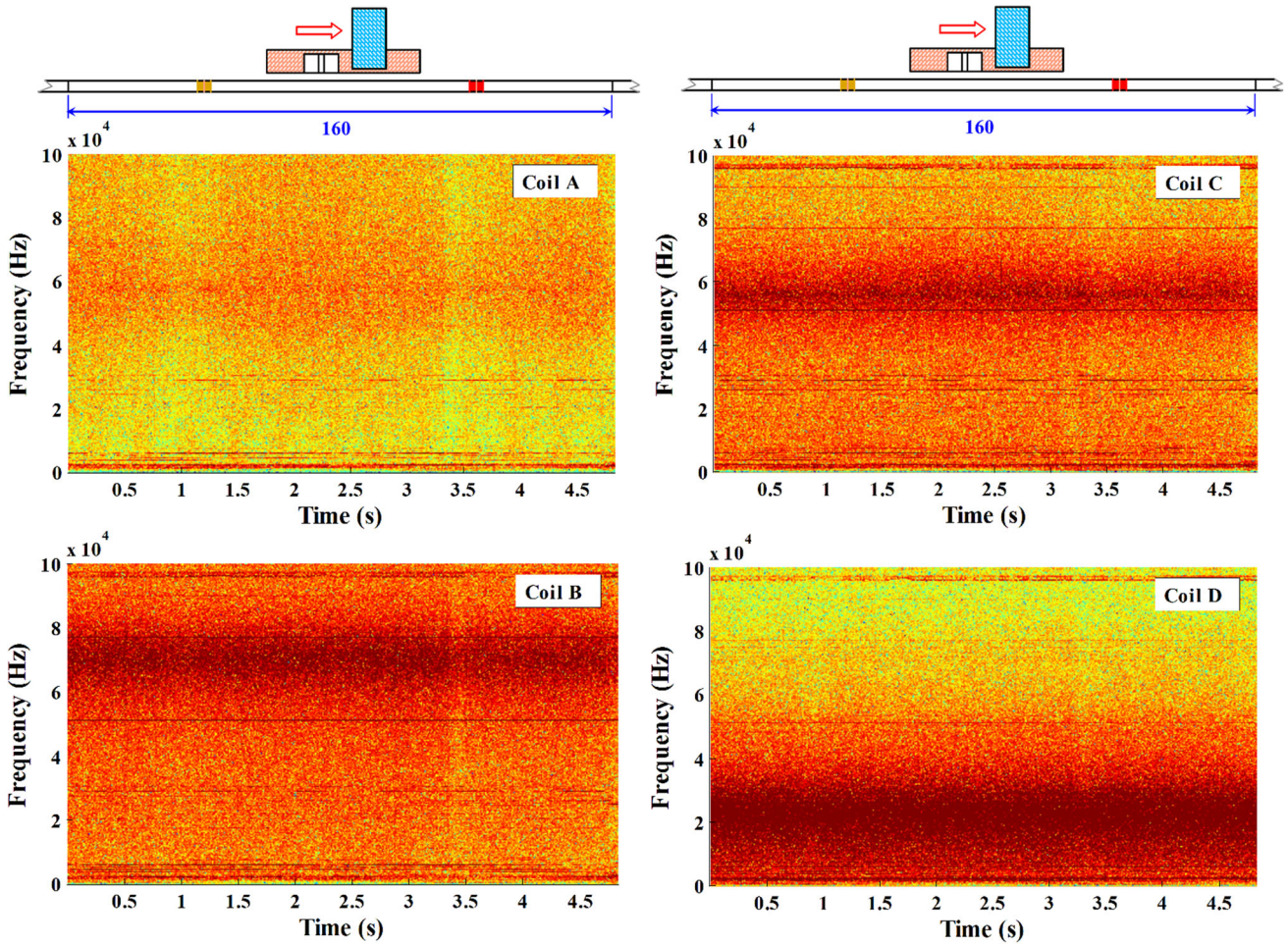

Fig. 7 Spectrograms of CMBN signals. Results obtained using four different coils and one magnet in the probe with a scanning speed v = 33 mm/s

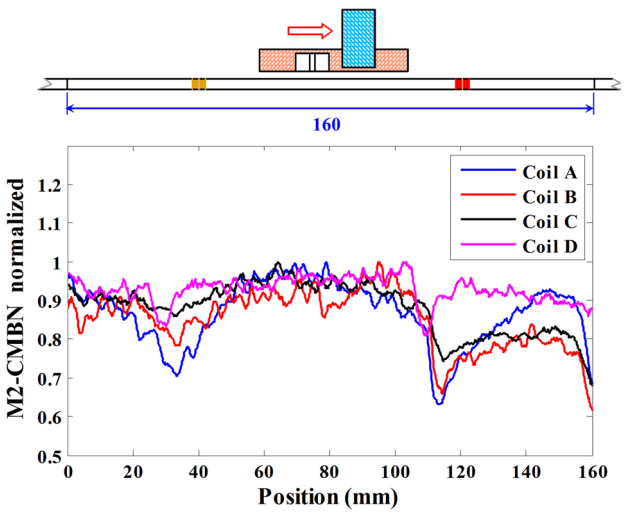

Fig. 8 Normalized variation in $M2_{CMBN}$ along the sample with a 30–100 kHz analysis band. Results obtained using four different coils and one magnet in the probe with a scanning speed v = 33 mm/s

the contact stresses concepts [23], the amplitudes of the loads used in the experiments of this work (88.3 and 107.9 kN) exceed 20 times the value of the load that reaches the material yield stress. In this condition and according to results of other studies analyzing the elastic-plastic behavior of surfaces under contact loading [24–26], in the sample analyzed in the present study were induced plastic deformations with relatively high amplitudes and accompanied mainly by compressive residual stresses.

The relatively high dislocation densities generated by plastic deformation are known to act as strong pinning sites for magnetic domain walls. In addition, in positive magnetostrictive materials such as steel, compressive residual stresses are known to decrease the 180° domain wall population in the direction longitudinal to the stress (i.e., along the length of the sample, or the same direction in which the CMBN was measured). Both these effects cause a reduction in Barkhausen activity.

Figure 9 shows the results when the coil was used behind the magnet and in front of it. Better results, i.e., greater sensi-

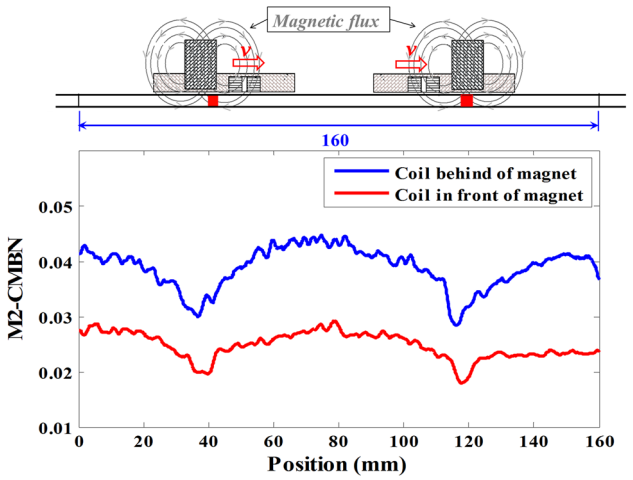

Fig. 9 Variation in $M2_{CMBN}$ along the sample with a 30–100 kHz analysis band. Results obtained using coil A and one magnet in the probe with a scanning speed v= 33 mm/s

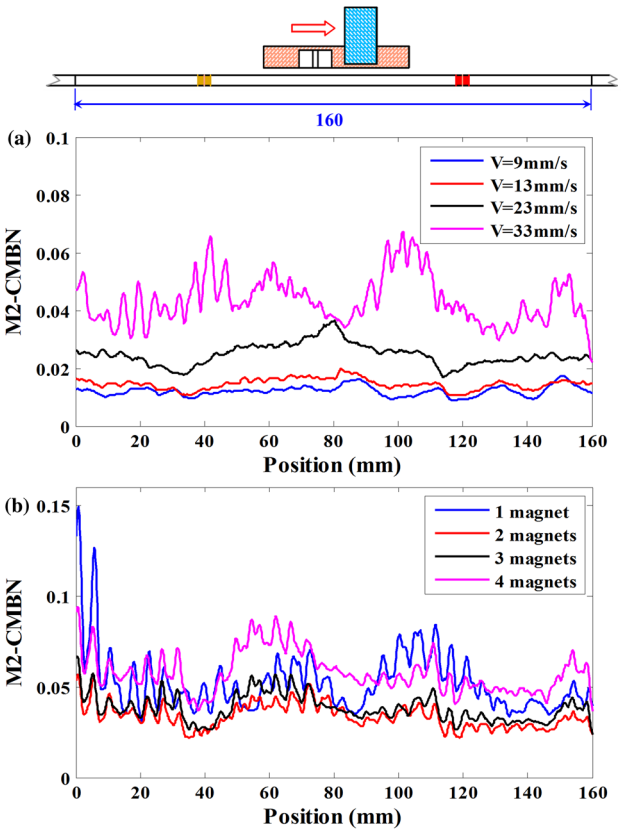

Fig. 10 Variation in $M2_{CMBN}$ along the sample with a 1–100 kHz analysis band. **a** Results obtained using coil A and one magnet in the probe with four different scanning speeds. **b** Results obtained using coil A and four different applied magnetic fields with a scanning speed v = 33 mm/s

tivity and a greater-amplitude signal, were obtained with the coil behind the magnet. This behavior can be attributed primarily to the dynamics of the magnetization/demagnetization of the steel when the signal is read. When the coil is in front of the magnet, the material is only subjected to a downward magnetic flux directed toward the left before it is scanned by the coil (see the magnetic flux lines in the schematic diagram in Fig. 9), while in the second case, when the coil is behind the magnet, the material is subjected to magnetic fluxes in opposite directions before it is scanned by the coil. As the CMBN signal is influenced by variations in the amplitude and direction of the magnetic field, the magnetic conditions in the material in the second case are more favorable for the generation of Barkhausen noise.

3.2 The Effect of Scanning Speed and Applied Magnetic Field

The effect of scanning speed and magnetic field were analyzed using the CMBN probe with coil A behind the magnet.

Figure 10 shows the effect of both parameters on $M2_{CMBN}$ when a 1–100 kHz frequency band was used. The results in Fig. 10a were obtained using four different scanning speeds and one magnet in the probe, while in Fig. 10b four different magnetic fields were applied and a scanning speed v = 33 mm/s was used. As in Fig. 6, most of the curves in Fig. 10 show that when calculating $M2_{CMBN}$ using a 1–100 kHz frequency band, there is no clear correlation between $M2_{CMBN}$ and the positions of the imposed plastic deformation. In contrast, in the spectrograms in Fig. 11, time bands corresponding to the positions of the plastic deformations can be clearly identified. Although the spectrograms in this figure correspond to only three combinations of scanning speed and applied magnetic field, similar behavior was observed in the spectrograms for all the combinations of magnetic fields and scanning speeds studied. The poor results shown in Fig. 10 are caused by low-frequency (1–30 kHz) stationary (interference) signals. This can be confirmed in Fig. 12, which shows the normalized variation in $M2_{CMBN}$ along the sample when a 30–100 kHz frequency band is used. There is a clear improvement in performance for all measurement conditions; the positions of the two plastic deformations can be clearly identified and their different amplitudes can be distinguished.

In Fig. 10, the amplitude of the CMBN signal increases slightly with increasing scanning speed. This is because an increase in scanning speed produces a proportional increase in the rate of change of the amplitude and direction of the magnetic flux inside the sample, in turn increasing the amplitude of the CMBN signal. In addition, in Fig. 12a, the normalized plot of $M2_{CMBN}$ shows that the sensitivity of the technique increases with increasing scanning speed. This represents an advantage when the technique is used in industrial applications as less time is required to scan for flaws.

In contrast, Fig. 12b shows that the magnetic field had a minimal influence on the sensitivity of the technique, and

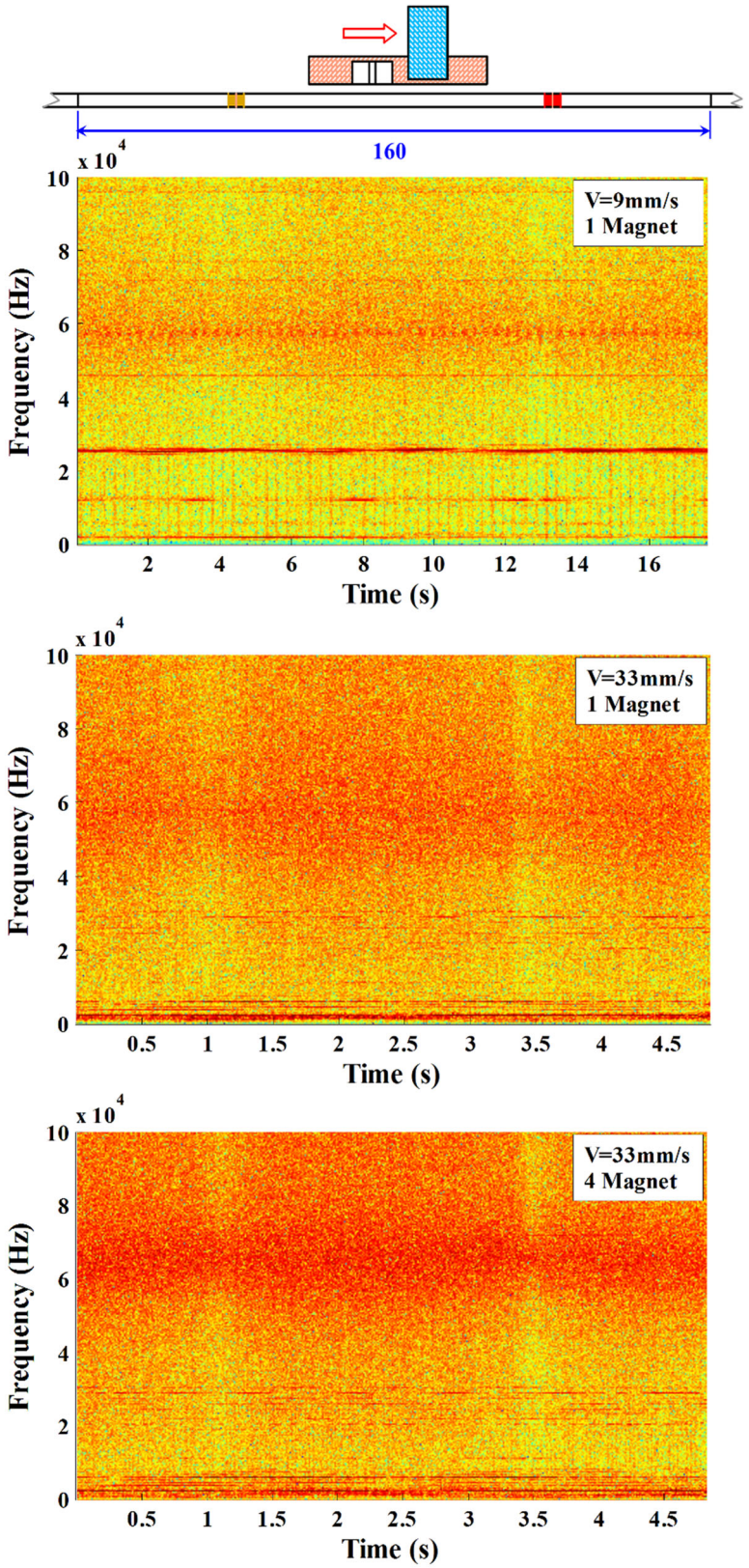

Fig. 11 Spectrogram of the CMBN signal. Results obtained using coil A

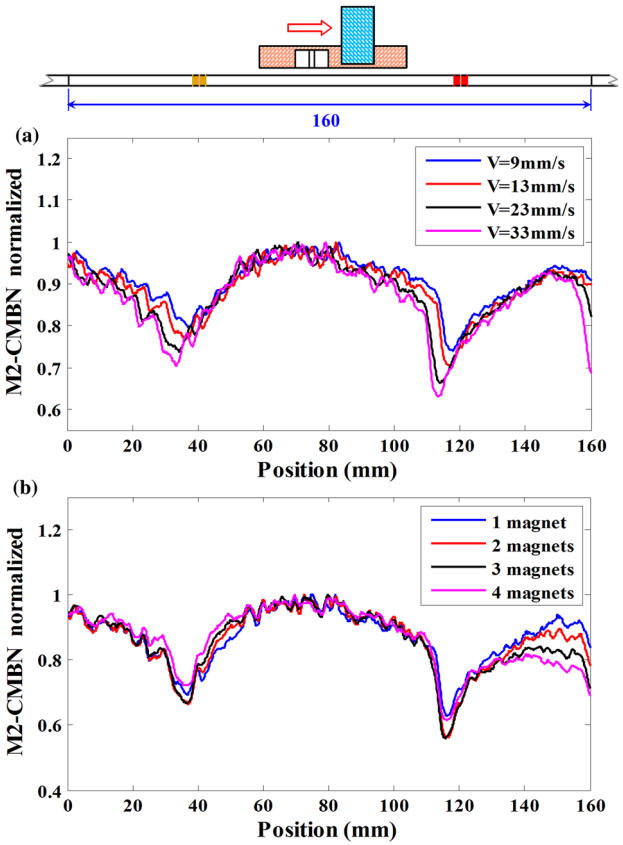

Fig. 12 Normalized variation in $M2_{CMBN}$ along the sample with a 30–100 kHz analysis band. **a** Results obtained using coil A and one magnet in the probe with four different scanning speeds. **b** Results obtained using coil A and four different applied magnetic fields with a scanning speed v = 33 mm/s

only small improvements were observed when two and three magnets were used. A possible explanation for this is that the magnetic field generated by the single magnet is sufficient to produce the Barkhausen noise. This is consistent with the activation of 180° domain walls, which usually requires only a low-amplitude magnetic field.

4 Conclusions

This paper has described the use of a non-destructive surface scanning technique for identifying plastic deformation zones based on continuous magnetic Barkhausen noise. The detection of plastic deformations produced by crushing stresses in a 1070 steel using the technique was analyzed. The influence of probe configuration, coil type, scanner speed, applied magnetic field and the frequency band used for the analysis on the effectiveness of the technique was studied. Filtering the raw signal in a 30–100 kHz bandpass filter before analyzing the time signal using a moving smoothing window based on a second-order statistical moment increased the effectiveness of the technique for all the conditions investigated.

The results show that the technique can be used to detect the position of plastic deformations and distinguish between their amplitudes and that its sensitivity depends on the type of coil, scanning speed and probe configuration but not on the applied magnetic field.

The factor that had the greatest influence on sensitivity was the type of coil used, the resonant frequency of the coil being the most important factor. For the conditions under which the experiments were carried out, when the coil has a resonant frequency within the frequency band being analyzed (in this case 1–100 kHz) it amplifies not only the CMBN signal but also interference, adversely affecting the quality of the signal. Coil A was the only coil whose resonant frequency was above the frequency band analyzed and was the one that showed the best sensitivity in terms of flaw detection. The best results were obtained using this coil behind the magnet and the highest scanning speed (33 mm/s).

This new surface-scanning technique can be used as the basis for novel solutions to several industrial NDT problems. However, further studies focusing primarily on optimization of the probe itself are needed to improve the performance of the technique.

Acknowledgements The authors would like to thank the State of São Paulo Research Foundation FAPESP (Ref. No. 05/57146-0).

References

1. Augustyniak, M., Augustyniak, B., Piotrowski, L., Chmielewski, M.: Determination of magnetisation conditions in a double-core Barkhausen noise neasurement set-up. J. Nondestruct. Eval. **34**, 16 (2015)
2. Vourna, P., Ktena, A., Tsakiridis, P.E., Hristoforou, E.: A novel approach of accurately evaluating residual stress and microstructure of welded electrical steels. NDT&E Int. **71**, 33–42 (2015)
3. Stupakov, O., Melikhov, Y.: Influence of magnetizing and filtering frequencieson Barkhausen noise response. IEEE Trans. Magn. **50**, 4 (2014)
4. Barkhausen, H.: Zwei mit hilfe der neuen verstarker entdeckte erscheinugen. Physik Z **20**, 401–3 (1919)
5. Jiles, D.C.: Dynamics of domain magnetization and the Barkhausen effect. Czech J. Phys. **50**, 893–988 (2000)
6. Pal'a, J., Bydzovsky, J.: Barkhausen noise as a function of grain size in non-oriented FeSi steel. Measurement **46**, 866–870 (2013)
7. Anglada-Rivera, J., Padovese, L.R., Capo-Sanchez, J.: Magnetic Barkhausen Noise and hysteresis loopin commercial carbon steel: influence of applied tensile stress and grain size. J. Magn. Magn. Mater. **231**, 299–306 (2001)
8. Ranjan, J., Jiles, D.C.: Magnetic properties of decarburized steels: an investigation of the effects of grain size and carbon content. IEEE Trans. Magn. **23**, 1869–1876 (1987)
9. Saquet, O., Chicois, J., Vincent, A.: Barkhausen noise from plain carbon steels: analysis of the influence of microstructure. Mater. Sci. Eng. A **269**, 73–82 (1999)

10. Mandache, C., Krause, T.W., Clapham, L.: Investigation of optimum field amplitude for stress dependence of magnetic barkhausen noise. IEEE Trans. Magn. **43**, 3976–3983 (2007)
11. Ding, Song, Tian, GuiYun, Dobmann, Gerd, Wang, Ping: Analysis of domain wall dynamics based on skewness of magnetic Barkhausen noise for applied stress determination. J. Magn. Magn. Mater. **421**, 225–229 (2017)
12. Franco, F.A., González, M.F.R., Campos, M.F., Padovese, L.R.: Relation between magnetic Barkhausen noise and hardness for Jominy quench tests in SAE 4140 and 6150 steels. J. Nondestruct. Eval. **32**, 93–103 (2013)
13. Kleber, X., Vincent, A.: On the role of residual internal stresses and dislocations on Barkhausen noise in plastically deformed steel. NDT&E Int. **37**, 439–445 (2004)
14. Dhar, A., Clapham, L., Atherton, D.L.: Influence of uniaxial plastic deformation on magnetic Barkhausen noise in steel. NDT&E Int. **34**, 507–514 (2001)
15. Crouch, A.E., Beuker, T.: In-line stress measurement by the continuous Barkhausen method. In: Proceedings of IPC 2004, International Pipeline Conference Calgary, Alberta, Canada (2004)
16. Crouch, A.E., Burkhardt, G.L.: System and Method for In-Line Stress Measurement by Continuous Barkhausen method. United States patent US 7,038,444 B2 (2006)
17. Franco, F.A., Padovese, L.R.: NDT flaw mapping of steel surfaces by continuous magnetic Barkhausen noise: volumetric flaw detection case. NDT&E Int. **42**, 721–728 (2009)
18. Caldas-Morgan, M., Padovese, L.R.: Fast detection of the magnetic easy axis on steel sheet using the continuous rotational Barkhausen method. NDT&E Int. **45**, 148–155 (2012)
19. Tumanski, S.: Induction coil sensors—a review. Meas. Sci. Technol. **18**, R31–R46 (2007)
20. Capó Sánchez, J., Padovese, L.: Magnetic Barkhausen noise measurement by resonant coil method. J. Magn. Magn. Mater. **321**, L57–L62 (2009)
21. Vashista, M., Moorthy, V.: Influence of applied magnetic field strength and frequency response of pick-up coil on the magnetic barkhausen noise profile. J. Magn. Magn. Mater. **345**, 208–214 (2013)
22. Morthy, V.: Important factors influencing the magnetic Barkhausen noise profile. IEEE Trans. Magn. **52**(4), 1–3 (2016)
23. Budynas, R.G., Nisbett, J.K., Shigley, J.E.: Shigley's Mechanical Engineering Design, 9th edn. McGraw-Hill, New York (2011)
24. Dumas, G., Baronet, N.: Elastoplastic indentation of a half-space by an infinitely long rigid circular cylinder. Int. J. Mech. Sci. **13**, 519–530 (1971)
25. Gao, Y.F., Bower, A.F., Kim, K.-S., Lev, L., Cheng, Y.T.: The behavior of an elastic-perfectly plastic sinusoidal surface under contact loading. Wear **261**, 145–154 (2006)
26. Bryant, M.J., Evans, H.P., Snidle, R.W.: Plastic deformation in rough surface line contacts—a finite element study. Tribol. Int. **46**, 269–278 (2012)